Development of the Morphology and Crystalline State due to Hybridization of Reinforced Toughened Nylon Containing a Liquid-Crystalline Polymer

SREEKUMAR PISHARATH,[1] **SHING-CHUNG WONG**[2]

[1]School of Materials Engineering, Nanyang Technological University, Nanyang Avenue,
Singapore 639798, Republic of Singapore

[2]Department of Mechanical Engineering and Applied Mechanics, North Dakota State University,
Fargo, North Dakota 58105

Received 22 April 2002; revised 20 December 2002; accepted 20 December 2002

ABSTRACT: A hybrid composite consisting of rubber-toughened nylon-6,6, short glass fibers, and a thermotropic liquid-crystalline polymers (LCP) was investigated by the LCP content being varied. The thermal behavior, morphology, and crystallization behavior due to hybridization were studied by differential scanning calorimetry (DSC), dynamic mechanical analysis (DMA), scanning electron microscopy (SEM), Fourier transform infrared (FTIR) spectroscopy, and wide-angle X-ray scattering (WAXS). DSC results indicated that the crystallinity of the glass-fiber-reinforced toughened nylon-6,6 was reduced by LCP addition, particularly 5–10 wt % LCP. DMA data showed that the miscibility between the blended components was maximum at the 5 wt % LCP composition, and the miscibility decreased with increasing LCP content. SEM photomicrographs revealed information consistent with the thermal behavior on miscibility. It was also observed that the 10 wt % LCP composition showed predominantly an amorphous character with FTIR and WAXS. WAXS results indicated that LCP hybridization increased the interplanar spacing of the hydrogen-bonded sheets of the nylon crystals rather than the spacing between the hydrogen-bonded chains. © 2003 Wiley Periodicals, Inc. J Polym Sci Part B: Polym Phys 41: 549–559, 2003

Keywords: liquid-crystalline polymers (LCP); hybrids; composites; morphology; crystallinity

INTRODUCTION

Elastomeric inclusions in thermoplastic matrices have been studied extensively in recent years.[1–3] The primary role of rubber particles is to relieve stress triaxiality at the crack tip through internal cavitations,[3] thereby promoting toughening mechanisms such as shear deformation in the matrix ligaments. However, rubber toughening sacrifices vital material properties, such as modulus, hardness, and strength. Reinforcing toughened matrices with short glass fibers has been introduced as a strategy[4,5] to counter the detrimental effect on mechanical stiffness due to rubber toughening. The advantages of fiber reinforcement are twofold: (1) it offsets the loss of mechanical properties such as the strength, stiffness, and heat deflection temperature and (2) it promotes fiber-induced toughening mechanisms in the matrix.[6,7]

The presence of inorganic fillers, however, raises the melt viscosity of polymers, resulting in lower processability and high energy consumption. Glass fibers also catalyze the tear and wear

---

Correspondence to: S.-C. Wong (E-mail: josh.wong@ndsu.nodak.edu)

Journal of Polymer Science: Part B: Polymer Physics, Vol. 41, 549–559 (2003)

of processing machinery. The feasibility of reprocessing glass-fiber-reinforced thermoplastics is unclear because of extensive fiber breakage during extrusion compounding. The hybridization of thermoplastics, glass fibers, and liquid-crystalline polymers (LCPs) has evoked considerable interest recently.[8] The LCP phase appears to enhance the processability of glass-fiber-reinforced toughened (GFRT) plastics, whereas the fiber length degradation can be minimized, and the fiber strengthening effect is consequently maximized. He et al.[9] reported synergistic properties for LCP/glass-fiber/thermoplastic hybrid composites.

An understanding on the thermoplastic materials containing an engineered combination of short glass fibers, LCPs, and elastomeric phases is lacking. In another article,[10] we reported the effect of LCP addition on the processability of GFRT nylon-6,6. However, the presence of rigid-rod LCPs also influences the morphology, melting behavior, crystallinity, and crystallization kinetics of the crystallizable components in the hybrid system. In general, the introduction of LCPs into LCP/thermoplastic blends is known to accelerate the rate of crystallization and enhance the crystallinity of thermoplastics.[11,12] However, the addition of LCPs was also found to limit the crystallization of thermoplastics, particularly for compatibilized thermoplastic/LCP blends.[13–15] In this article, we investigate the changes occurring in the crystal structure and morphology of GFRT nylon-6,6 with the addition of LCPs. A variety of analytical techniques, including differential scanning calorimetry (DSC), dynamic mechanical analysis (DMA), X-ray diffraction (XRD), Fourier transform infrared (FTIR), wide-angle X-ray scattering (WAXS), and scanning electron microscopy (SEM), were employed to elucidate the crystallization behaviors and morphological transformations in the hybrid composites.

EXPERIMENTAL

Processing

Rubber-toughened nylon-6,6 containing 20 vol % poly(ethylene–propylene–diene monomer) (EPDM; Zytel ST801, DuPont) was dry-blended with 20 wt % glass fibers (length = 12 mm, diameter = 17 μm) and independently with 5, 10, and 20 wt % LCP (Vectra A950, Hoechst Celanese). The LCP was 27 mol % 2-hydroxy-6-naphthoic acid and 73 mol % *p*-hydroxybenzoic acid. The dry blended resins were melt-mixed with a high-shear-rate, intermeshing, corotating twin-screw extruder (Leistritz Micro 18; screw diameter = 18 mm). The temperature profile in the extruder was 260–280–285–285–292 °C. The screw speed was kept at 200 rpm. The extruded pellets were injection-molded into 3.5-mm-thick dog-bone specimens with a Battenfeld BA 300 CD$^{\text{Plus}}$ injection-molding machine. The temperatures in zone 1 and zone 2 of the barrel for injection molding were 285 and 292 °C, respectively. The nozzle temperature was 275 °C, and the mold was kept at the ambient temperature. An injection pressure of 70 bar and a holding time of 50 s were used. The screw speed was kept at 140 rpm. All materials were dried at 80 °C for at least 72 h in a vacuum oven before processing.

DSC Analysis

A TA Instruments differential scanning calorimeter (DSC 2920) equipped with TA thermal analysis software was used for calorimetric studies. Samples weighing around 7 mg were cut from the injection-molded samples, and all experiments operated with a stream of nitrogen. The sample was first heated from room temperature to 310 °C at a rate of 20 °C min^{-1} and kept at that temperature for 10 min to erase the thermal history. The sample was then cooled to room temperature at a rate of 10 °C min^{-1}. The cooled sample was reheated to 300 °C at a rate of 10 °C min^{-1}. The peak maximum corresponded to the melting/crystallization temperature, and the area under the thermogram provided the heat of crystallization/fusion.

Dynamic Mechanical Properties

DMA was performed with a TA DMA 2980 equipped with TA thermal analysis software. The measurements were made on injection-molded plaques at a scan rate of 3 °C min^{-1} and at a frequency of 1 Hz in a temperature range of 25–200 °C. A double cantilever clamp in a bending mode was used for the tests.

WAXS

XRD measurements were conducted on injection-molded plaques with a Shimadzu Lab XRD-6000 X-ray diffractometer employing Ni-filtered Cu Kα radiation (λ = 1.54 Au) operating at 50 kV and 20

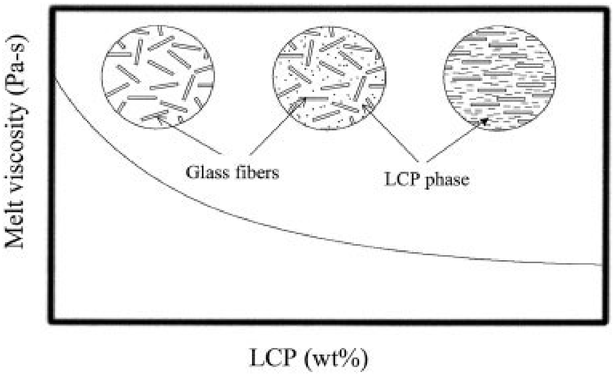

Figure 1. Schematic showing the effect of the LCP on the melt viscosity of fiber-reinforced thermoplastics from ref. 10. The evolution of the morphology with the addition of the LCP is described in the smaller, circled figures.

mA. We obtained the scans in a continuous scan mode by counting for 6 s at 0.1° steps ($\theta/2\theta$ scan). The scanning range was restricted between 10.00 and 35.00° so that we could observe the relevant peaks pertaining to nylon-6,6.

FTIR Spectroscopy

A fine powder of an injection-molded plaque was made by the pulverization of the specimen in a Fritsch Pulverisette 14 rotor mill. The powder was mixed with KBr and made into thin plates 13 mm in diameter and approximately 1 mm thick in a hydraulic press. Measurements were performed on these compressed samples with a PerkinElmer 2000 FTIR spectrophotometer with a resolution of 4 cm^{-1}.

Microscopy

A JEOL 5410 LV model SEM instrument was used to analyze the dispersed phase morphology of the samples. For this purpose, the injection-molded specimens were cryofractured in liquid nitrogen, and the fracture surfaces coated with gold in an SPI sputter coater were observed with SEM.

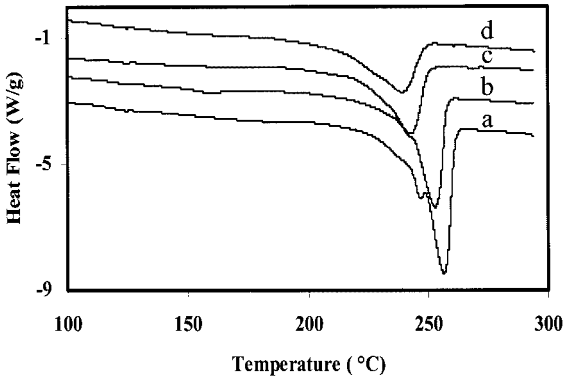

Figure 2. DSC thermograms of the second heating scan for GFRT nylon-6,6 containing (a) 0 wt % LCP, (b) 5 wt % LCP, (c) 10 wt % LCP, and (d) 20 wt % LCP.

RESULTS AND DISCUSSION

Thermal Behavior

Figure 1 shows a schematic illustrating the effect of LCP addition on the processability of glass-fiber-containing polymers.[10] Clearly, the addition of LCP to the glass-fiber-reinforced composite reduces the melt viscosity and energy consumed during extrusion, as represented by the total torque for a given amount of the composite material. Table 1 shows the crystallization and melting temperatures for GFRT nylon-6,6 and LCP hybrid composites. The DSC thermograms of GFRT nylon-6,6 with increasing LCP content for the second heating scan are plotted in Figure 2. Note that the peaks under focus are those that

Table 1. Thermal Analysis Data of the GFRT Nylon-6,6 and Their LCP-Containing Hybrid Composites

Sample	T_m (°C)[a]	T_c (°C)[b]	$T_m - T_c$ (°C)	T_m (°C)[c]	ΔH_f (J/g)
GFRT nylon-6,6	261.4	230.0	31.4	256.7	44.1
GFRT nylon-6,6 + 5 wt % LCP	261.4	226.7	35.7	253.1	42.3
GFRT nylon-6,6 + 10 wt % LCP	261.8	214.6	47.2	242.7	37.3
GFRT nylon-6,6 + 20 wt % LCP	262.0	212.0	50.0	240.0	35.6

[a] Melting temperature determined from the first heating cycle.
[b] Crystallization temperature determined from the first cooling cycle.
[c] Melting temperature determined from the second heating cycle.

belong to the nylon-6,6 component. In the first heating scan, there is no apparent change in the melting temperature and appearance of the thermogram. In the second heating scan, there are observable differences in the melting behavior of GFRT nylon-6,6 with increasing LCP content. The glass-fiber-reinforced composite [Fig. 2(a)] displays multiple melting peaks indicating the presence of polymorphic transformation in the crystal of nylon-6,6.[16] Of the melting peaks of polymorphs, the lower peak corresponds to the crystals formed during the first cooling cycle. The higher melting peak is formed by reorganization of the crystals during the second heating cycle. With increasing LCP content, the polymorphic transformation of nylon disappears. The melting temperatures of the LCP hybrids shift to lower values, and the melting transitions become broader. There is a pronounced drop by 10 °C in the melting point when the LCP content is increased from 5 to 10 wt %. For the higher LCP content at 20 wt %, the melting point depression levels off.

The shift in the melting temperature yields important information concerning the interaction behavior of LCP-containing polymer blends. For a binary mixture of two high molecular weight polymers, for example, one crystalline and the other amorphous, it is possible to determine the polymer–polymer interaction parameter by the application of the Nishi–Wang theory[17] to the melting point data. We have attempted to use this theory to understand the interactions between the nylon phase and the LCP. The Nishi–Wang theory is represented by the following equations:

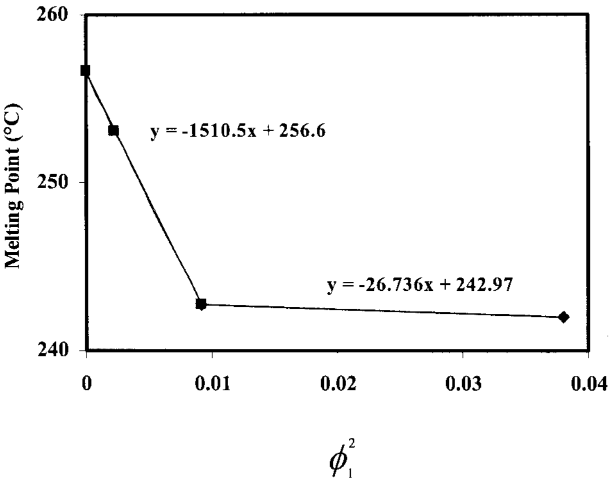

Figure 3. Melting point of GFRT nylon-6,6 versus ϕ_1^2.

Table 2. Conversion of the LCP Weight Fraction to the Volume Fraction

Composition	Weight Fraction (wt %)	Volume Fraction[b]
GFRT nylon-6,6[a] + 5 wt % LCP	0.05	0.048
GFRT nylon-6,6[a] + 10 wt % LCP	0.1	0.096
GFRT nylon-6,6[a] + 20 wt % LCP	0.2	0.194

[a] Zytel ST801 + 20 wt % glass fiber.

[b] Density of Zytel ST 801 = 1.183 g/cm^3; density of Vectra A950 = 1.400 g/cm^3; density of glass fiber = 2.873 g/cm^3.

$$T_{\mathrm{m}} = T_m^{\circ} + T_m^{\circ}\left(\frac{V_2}{\Delta H_2}\right)B\phi_1^2 \tag{1}$$

$$B = \chi_{12}\frac{RT}{V_1} \tag{2}$$

where ϕ_1 is the volume fraction of LCP, B is the polymer–polymer interaction energy density, T_m° is the melting temperature of GFRT nylon-6,6 without the LCP, T_{m} is the melting temperature of GFRT nylon-6,6 in the LCP blends, $\Delta H_2/V_2$ is the heat of fusion per unit volume of 100% crystalline toughened nylon-6,6 with glass reinforcements, V_1 is the molar volume of LCP, χ_{12} is the Flory–Huggins interaction parameter, R is the gas constant, and T is the temperature.

As indicated in eq 1, the slope of a plot of the melting point of GFRT nylon-6,6 in the LCP blends versus ϕ_1^2 could indicate the intensity of the polymer–polymer interaction, χ_{12}, at a given temperature and ϕ_1 value. It is understood that the more negative χ_{12} is, the better the polymer–polymer miscibility is. Data on the values of $\Delta H_2/V_2$ are unavailable in this study. All other quantities other than χ_{12} are positive in magnitude. Figure 3 shows the melting point variation versus ϕ_1^2. Table 2 shows the conversion of the weight fraction of the LCP to the volume fraction, which depends on the densities of components in the hybrid. As evident from Figure 3, the slope of variation in the melting temperature is most negative in the range of 0.05–0.1 vol % LCP (corresponding to 5–10 wt % LCP). At higher volume fractions, the slope levels off, and this suggests that the interaction arising from LCP introduction has been reduced. From the slopes in Figure

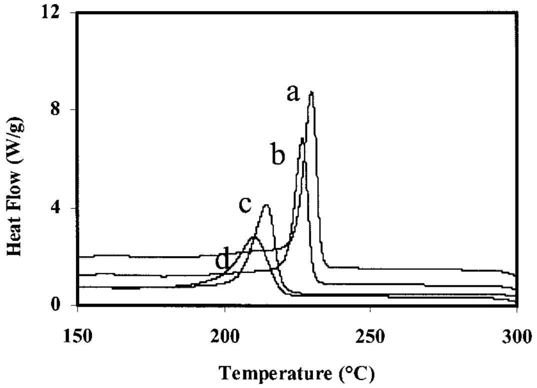

Figure 4. DSC thermograms of the first cooling scan for GFRT nylon-6,6 containing (a) 0 wt % LCP, (b) 5 wt % LCP, (c) 10 wt % LCP, and (d) 20 wt % LCP.

3, we qualitatively deduce that from 5 to 10 wt % LCP, the polymer–polymer interaction is most intense, whereas the interaction decreases at higher LCP contents. Zheng et al.[18] made a similar observation in a study of miscibility and phase separation in polymer blends.

Figure 4 shows the cooling thermograms of GFRT nylon-6,6 and its blends with the LCP. As for the melting point variation, the crystallization temperature decreases steadily after 5 wt % LCP. The degree of supercooling (ΔT), which is defined as the difference between the peak melting temperature and the crystallization temperature, can be used to characterize the crystallization behavior of polymer blends. The greater ΔT is, the higher the retardation is in the crystallization process of the polymer. Figure 5 shows the plot of ΔT variation with the LCP content. The ΔT value increases with the LCP content, and this indicates that the crystallization process of GFRT nylon-6,6 is depressed in the blends by the introduction of the LCP. Such behavior has been observed in polymer blends when the compatibility between the blended components is improved.[19,20]

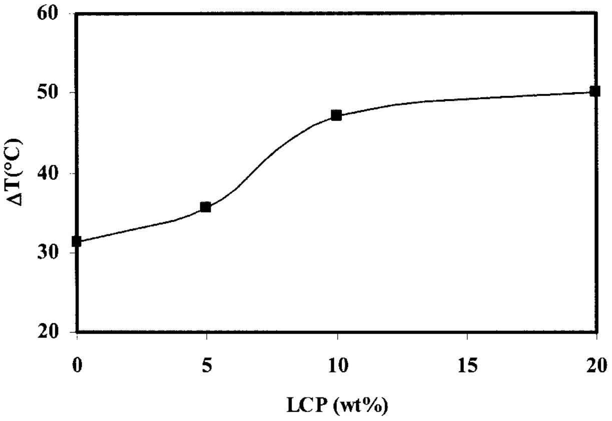

Figure 5. ΔT versus the LCP content.

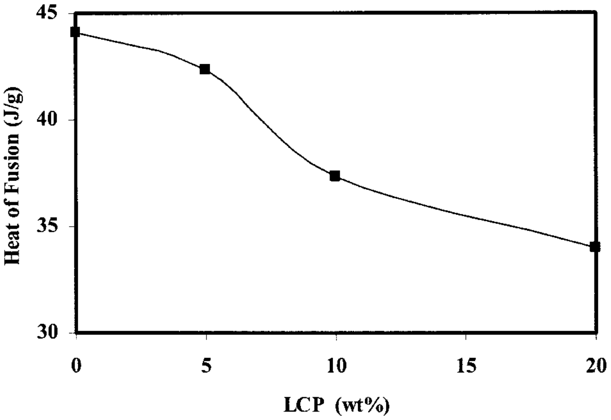

Figure 6. Heat of fusion normalized against GFRT nylon-6,6 versus the LCP content.

The heat of fusion is denotative of the crystallinity inherent in the samples. Because of the unavailability of the data on the heat of fusion of 100% crystalline GFRT nylon-6,6, we were unable to calculate the relative values of crystallinity for each composition. However, the heat of fusion of pure LCP was found to be very small (2 J/g). Therefore, its contribution to the total heat of fusion of the hybrid could be neglected without significant error being introduced to the trend observed. Figure 6 shows the variation in the heat of fusion normalized against the content of GFRT nylon-6,6 in the blends obtained from the second heating scan. The heat of fusion markedly decreases from 42 J/g at 5 wt % LCP to 37 J/g at 10 wt % LCP. Clearly, the degree of crystallinity of GFRT nylon-6,6 is severely reduced by the addition of LCP, especially in the range of 5–10 wt % LCP.

It is well known that the crystallization and melting of crystallizable components of a blend are largely affected by the interchange reactions between the component polymers during melt mixing.[21] The most favorable interchange reaction that may take place in the blend between nylon-6,6 and polyester (VA 950) is acidolysis[22] between the carboxyl groups on nylon chains and the ester groups on the LCP. In this work, we used a commercially available toughened nylon-6,6, Zytel ST801, which is a graft-copolymer-toughened nylon containing 20 vol % EPDM rub-

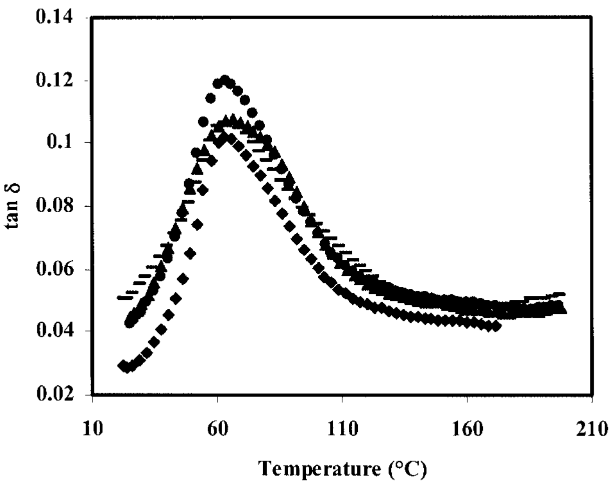

Figure 7. Tan δ versus the temperature for GFRT nylon-6,6 containing (◆) 0 wt % LCP, (▲) 5 wt % LCP, (●) 10 wt % LCP, and (–) 20 wt % LCP.

ber particles. The chemical structure of this graft copolymer is not known. We surmise that this graft copolymer plays a role in compatibilization and facilitates the interaction between the glass-fiber-reinforced nylon-6,6 and Vectra A950.

Compatibilizing agents are generally graft or block copolymers with reactive chemical structures for those polymers being blended.[23] Seo et al.[24] found that a third component in the form of a maleic anhydride-grafted ethylene–propylene terpolymer facilitated the structural development of the LCP in nylon-4,6. They also observed[25] that maleated EPDM could function as an efficient compatibilizer for nylon-6 and Vectra A950. All these findings reiterate the possible role of EPDM in enhancing the miscibility between toughened nylon-6,6 and LCP.

Dynamic Mechanical Properties

Figure 7 shows the variation of the α-peak relaxation spectra with temperature for GFRT nylon-6,6 and its blends with the LCP. Despite DMA being a sensitive technique, no transition peaks pertaining to Vectra A950 are observable. Vallejo et al.[26] could not observe the glass-transition temperature (T_g) of Vectra A950 in the blends of two thermotropic LCPs because of the low and broad range of the glass transition. The α-peak corresponds to the glass transition resulting from the initiation of micro-Brownian motion of the amorphous chains. Figure 7 shows that T_g of GFRT nylon-6,6 (63 °C) increases marginally by 3 °C to 66 °C with an addition of 5 wt % LCP, revealing some miscibility between the blended components. The magnitude of this increase is more than that predicted by Fox's equation for perfectly miscible blends. In other compositions, T_g is nearly the same as that of the GFRT nylon-6,6. Moreover, the 5 wt % LCP hybrid shows the broadest α-peak transition of all the compositions, suggesting better interaction between the polymer components. Tjong and Meng[27] observed a similar broad transition in blends of nylon-6 and LCP. They attributed this broadened peak to the good interaction between the nylon and LCP phases.

The difference in the miscibility between the blends can be observed clearly from the SEM photomicrographs of the cryofractured injection-molded plaques. Figure 8 shows the SEM photomicrographs of GFRT nylon-6,6 containing 5, 10, and 20 wt % LCP. All photomicrographs were taken from the core region. In the 5 wt % composition [Fig. 8(a)], the LCP phase cannot be distinguished from the matrix because of the good miscibility between the toughened nylon and LCP domains, at least at the level of magnification used here. In the 10 wt % LCP hybrid [Fig. 8(b)], the LCP phase can be distinguished as spherical droplets of 0.5–0.7 μm. When the LCP content is further increased to 20 wt % [Fig. 8(c)], the size of the dispersed droplets increases to 2 μm. The SEM photomicrographs indicate that the 5 wt % LCP composite exhibits the best miscibility of all the compositions studied, and this is consistent with the tan δ results in Figure 7. Figure 8(d) shows the skin region of the 20 wt % LCP composite. Some elongated fibrils of the LCP, approximately 2 μm long, can be observed, and they suggest diminished compatibility at higher LCP contents.

The intensity of the α peak is maximum for the GFRT nylon-6,6 with 10 wt % LCP, as shown in Figure 7. As stated previously, the transition associated with the α peak occurs in the amorphous region of the polymer with the initiation of micro-Brownian motion of the molecular chains. This implies that the magnitude of the α peak should be greater for an amorphous polymer than that of a semicrystalline polymer. It further indicates that the 10 wt % LCP hybrid is the least crystalline of all the studied compositions. This finding is also consistent with our deductions from the DSC data in Figures 2–6.

Figure 9 shows the variation of the storage modulus with temperature. The 20 wt % LCP

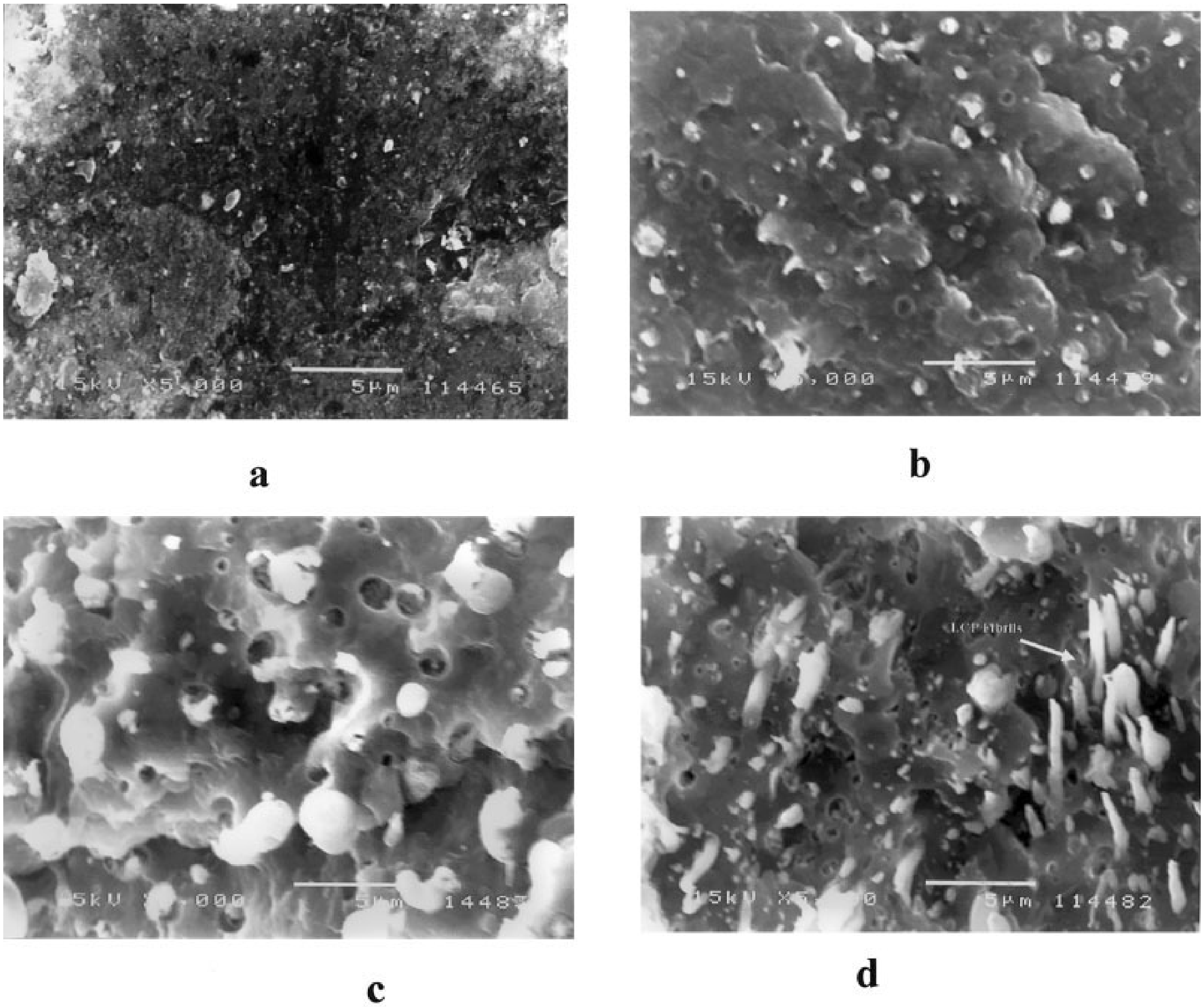

Figure 8. SEM photomicrographs of cryofractured samples of GFRT nylon-6,6 containing (a) 5 wt % LCP (in the core region), (b) 10 wt % LCP (in the core region), (c) 20 wt % LCP (in the core region), and (d) 20 wt % LCP (near the skin region). Regions displaying glass fibers are not shown in the photomicrographs.

hybrid composite exhibits the highest storage modulus over the whole range of temperatures. The improvement in the stiffness in the 20 wt % LCP hybrid is attributed to the microfibrillation of the LCP phase in the polymer matrix, as evident from the SEM photomicrograph [Fig. 8(d)]. In another article,[10] we reported that the 20 wt % LCP composite exhibited the highest tensile strength and modulus. The polymer–polymer interface apparently suffices to promote effective stress transfer from the matrix to the LCP fibrils at the beginning of elastic deformation, and this results in the stiffening effect.

However, the inclusion of 5 and 10 wt % LCP in GFRT nylon-6,6 impacts negatively on the stiffness. The 10 wt % LCP hybrid has the least stiffness of all the compositions. It is understood that compatibility between the matrix and LCP strengthens the interface, giving rise to stress transfer from the polymer matrix to the LCP fibrils and enhancing the load-bearing properties. However, the reinforcing effectiveness also depends on the filler aspect ratio and volume fraction. For a volume fraction that is too low, the deformation behavior is governed by matrix-dominant mechanisms, whereas filler-dominant fail-

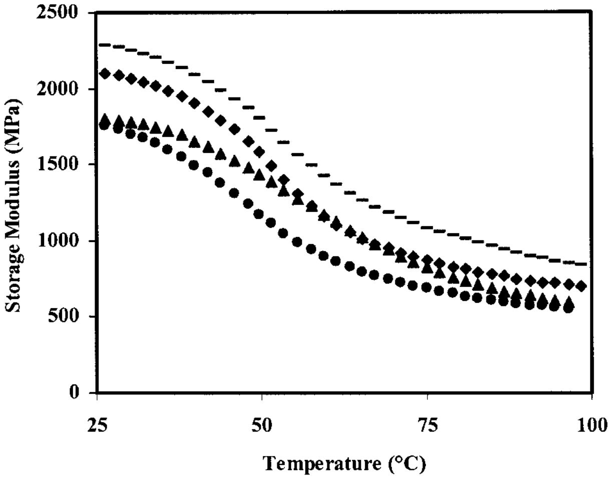

Figure 9. Storage modulus versus the temperature for GFRT nylon-6,6 containing (◆) 0 wt % LCP, (▲) 5 wt % LCP, (●) 10 wt % LCP, and (–) 20 wt % LCP.

ure only occurs when the critical filler volume fraction is reached. An increase in the filler volume fraction is directly translated to a decrease in the load-bearing matrix volume fraction when the critical filler volume fraction is not achieved. The dispersion of the LCP phase that creates droplet morphology would also induce stress concentration, promoting premature failure. This would turn out to be detrimental to the mechanical properties of the composite.[28,29] An examination of the SEM photomicrographs shows that the LCP phase could not clearly be distinguished in the 5 wt % composition [Fig. 9(a)] because of the good miscibility. In the 10 wt % LCP hybrid, the LCP phase exists as spherical droplets. We believe an insufficient LCP volume fraction and morphological factors, which include the droplet morphology of LCP, adversely influence the stiffness of the hybrid composites at 5 and 10 wt % LCP. As a result, the stiffening effect only occurs at 20 wt % LCP.

FTIR Spectroscopy

The technique of IR spectroscopy is also employed for measurements for the crystallization and orientation of polyamides.[30] It was reported[31] that the bands at 936 and 1199 cm^{-1} could be used to represent the crystalline phase of nylon-6,6. We adopt this method in a qualitative manner to assess the change in the crystalline state of GFRT nylon-6,6 with the addition of the LCP. Figure 10 shows the FTIR spectra of GFRT nylon-6,6 and its 5 and 10 wt % LCP composites. Both the GFRT nylon-6,6 and its 5% LCP hybrid display the 1199- and 936-cm^{-1} bands, which indicate the crystalline phase of nylon. However, for the 10 wt % LCP composite, the intensity of these bands becomes minimal. Surprisingly, the band at 924 cm^{-1}, representing the amorphous phase of nylon-6,6, cannot be detected. The IR observation also indicates that the crystallinity of GFRT nylon-6,6 with 10 wt % LCP is lower than that of the composite with 5 wt % LCP. This is consistent with our results from the thermal analysis, which shows that the introduction of the LCP slashes the degree of crystallinity in the nylon phase.

WAXS

XRD is widely used to analyze filled polymers by determining parameters such as the crystallinity and crystallite sizes of the matrix polymer.[30] WAXS has been employed to study the miscibility[32] and polymorphic transformation[33] in thermoplastic/LCP blends. In this article, we attempt to quantify the variation in the crystal size and perfection of crystallites of GFRT nylon-6,6 containing LCP with WAXS.

The stable crystal form of nylon-6,6 is the α structure.[30] Figure 11 shows the schematic of the crystal structure of nylon-6,6, showing the planes of interest. The chains in the α structure are in the fully extended planar zigzag conformation forming planar sheets of hydrogen-bonded molecules that, in turn, are stacked upon one another.[34] The planar sheets are also bonded to each other by hydrogen bonds. The crystal symmetry is triclinic, with one chemical unit per unit cell.

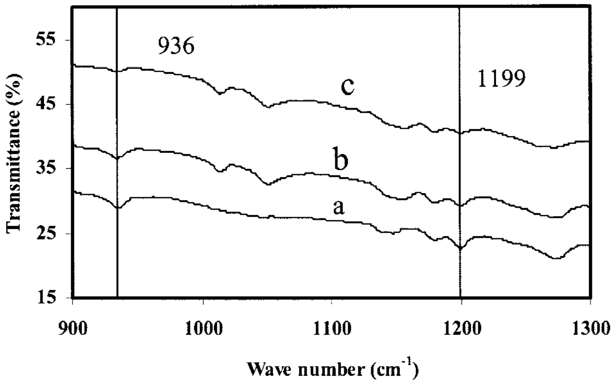

Figure 10. FTIR spectra of GFRT nylon-6,6 containing (a) 0 wt % LCP, (b) 5 wt % LCP, and (c) 10 wt % LCP.

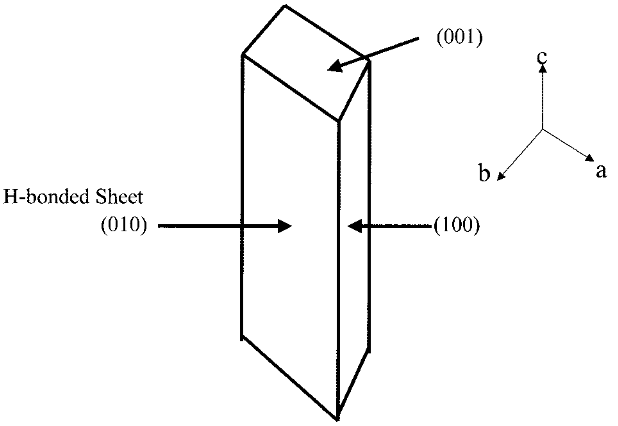

Figure 11. Schematic of the crystal structure of nylon-6,6 showing the (100), (010), and (001) crystallographic planes and the crystallographic axes. The (110) plane is the diagonal plane and is not shown.

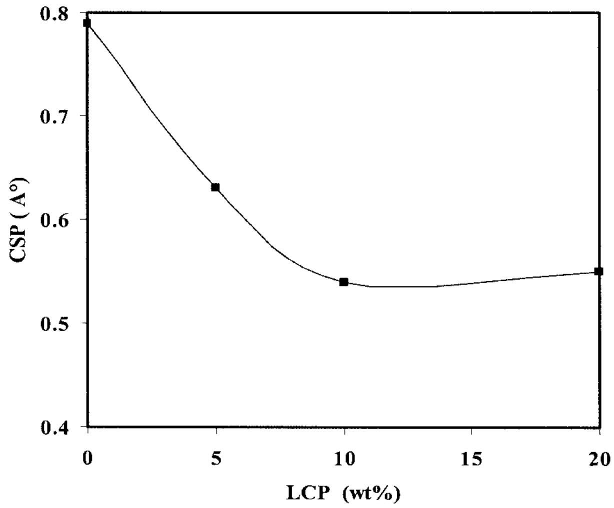

Figure 13. CSP values corresponding to the $\alpha 1$ peak versus the LCP content.

Figure 12 shows the XRD patterns of GFRT nylon-6,6 and its blends with the LCP. At room temperature, the intense equatorial reflection is from the (100) plane at $2\theta = 20.6°$, labeled $\alpha 1$, and from the (010) and (110) doublet at $2\theta = 23.3°$, labeled $\alpha 2$.[35,36] The width of the crystalline peak is inversely related to the size of the crystal. A measure of the crystallite size and perfection (CSP) can be defined with the Scherer equation:[30]

$$\mathrm{CSP} = \frac{k\lambda}{(\beta \cos 2\theta)} \tag{3}$$

where λ is the X-ray wavelength, β is the full width at half-maximum for the peak at 2θ, and k is a constant (0.9). For many polymers, a high CSP is associated with high crystal density.[30] Using the most prominent peak, we could calculate the CSP value from the (100) plane.

Figure 13 shows the variation of the CSP value for the (100) peak with the LCP content. There is a sudden decrease in the CSP value from 0.792 Au for GFRT nylon-6,6 to 0.538 for GFRT nylon-6,6 with 10 wt % LCP. After this region, the CSP value remains almost constant. The CSP value reinforces the notion that the introduction of LCP into GFRT nylon-6,6 reduces the crystallinity of the nylon phase.

McCullagh et al.[37] showed that the difference in the d-spacing between the blend components

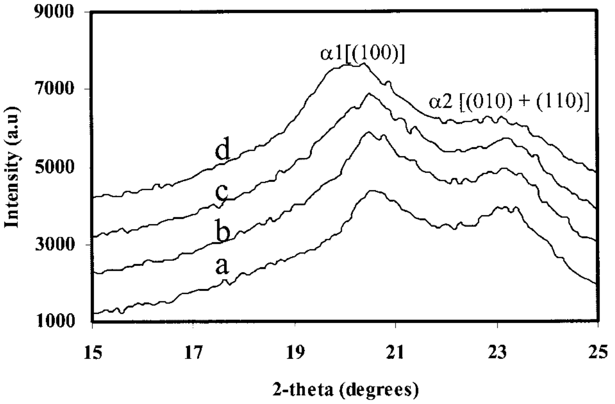

Figure 12. X-ray diffractograms of GFRT nylon-6,6 containing (a) 0 wt % LCP, (b) 5 wt % LCP, (c) 10 wt % LCP, and (d) 20 wt % LCP. $\alpha 1$ and $\alpha 2$ are the two intense equatorial reflections from the (100) and (010)+(110) planes, respectively. The intensity of the $\alpha 2$ peak decreases with increasing LCP content.

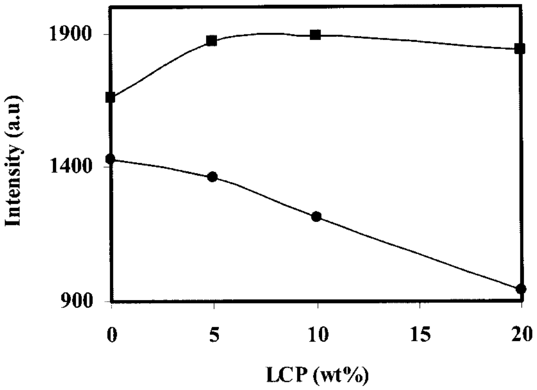

Figure 14. X-ray intensity versus the LCP content for (■) the $\alpha 1$ peak and (●) the $\alpha 2$ peak.

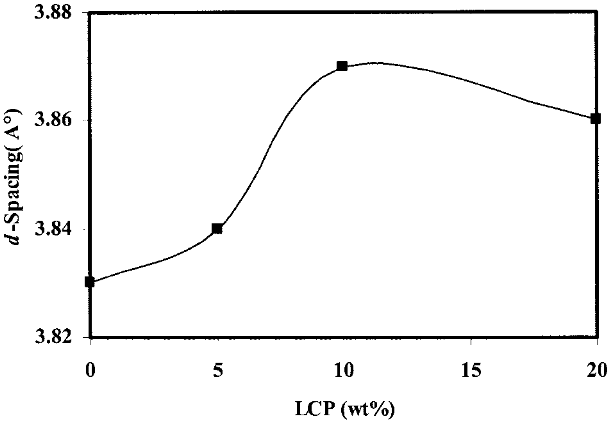

Figure 15. d-spacing values versus the LCP content for the $\alpha 2$ peak.

could be used as a tool to explain the transesterification between two thermotropic LCPs. In their study, an increase in the d-spacing between the blend components suggested enhanced interaction. We apply a similar rationale to assess any change in the d-spacing of GFRT nylon-6,6 with the addition of the LCP. As indicated in Figure 11, the peak at $2\theta = 20.6°$ arises from the distance between the hydrogen-bonded chains, and the peak at $2\theta = 23.3°$ occurs from the separation between the hydrogen-bonded sheets. The intensity of these equatorial Bragg reflections are governed by the perpendicular distance between the chains within the hydrogen-bonded sheet and the perpendicular distance between the hydrogen-bonded sheets themselves. Figure 14 shows the intensity variation of these two peaks with the LCP content. From the graph, it is clear that the intensity of the peak at $2\theta = 23°$ decreases and that the intensity of the peak at $2\theta = 20.6°$ remains steady with increasing LCP content. LCP blending evidently increases the interplanar spacing between the hydrogen-bonded sheets, rather than that of the spacing between the hydrogen-bonded chains. This larger spacing between the hydrogen-bonded sheets leads to enhanced mobility of the sheets in comparison with hydrogen-bonded chains. Figure 15 shows the variation in the d-spacing of the crystallographic planes corresponding to this peak ($2\theta = 23°$) as a function of the LCP content. As anticipated, the d-spacing value increases with the LCP content up to 10 wt % LCP and drops gently afterward. We believe that the increase in the d-spacing in the 5 and 10 wt % LCP hybrids is indicative of the enhanced polymer–polymer interaction leading to good miscibility. If only the interfacial interaction is taken into consideration, then the 5 wt % LCP composition is expected to yield the maximum d-spacing. In contrast, the 10 wt % LCP yields the maximum d-spacing. This could be caused by the combined effects of enhanced amorphous character and interfacial interaction between the nylon domains and LCP phase in the 10 wt % LCP hybrid. Supportive evidence referring to the amorphous character of the 10 wt % LCP hybrid awaits future studies.

CONCLUSIONS

The effects of hybridization on the crystallization and crystalline state were studied with different analytical techniques. The sample materials were complex, and the data were detailed. Blending LCPs with GFRT nylon-6,6 dramatically altered the crystalline nature of the nylon phase. DSC and DMA results indicated that an increase in the LCP content reduced the crystallinity of GFRT nylon-6,6. DMA data showed that the 5 wt % LCP hybrid was most miscible between the nylon and LCP domains of all compositions and that the 10 wt % hybrid yielded an amorphous morphology. The latter was determined with FTIR and XRD techniques. The XRD results also suggested that blending GFRT nylon-6,6 with the LCP enlarged the spacing between hydrogen-bonded sheets of the nylon crystal but not the hydrogen-bonded chains. This led to higher mobility of the hydrogen-bonded sheets in comparison with that aligned with the hydrogen-bonded chains. Future work will focus on comparative studies of samples with and without fibers and with and without elastomers. Additional data can also be derived to precisely establish the effects of hybridization on crystallization kinetics.

REFERENCES AND NOTES

1. Bucknall, C. B. Toughened Plastics; Applied Science: London, 1977.
2. Oshinski, A.; Keskkula, H.; Paul, D. R. Polymer 1992, 33, 268–283.
3. Bucknall, C. B. In Polymer Blends; Paul, D. R.; Bucknall, C. B., Eds.; Wiley: New York, 2000.
4. Laura, D. M.; Keskkula, H.; Barlow, J. W.; Paul, D. R. Polymer 2001, 42, 6161–6172.
5. Sui, G. X.; Wong, S. C.; Yue, C. Y. Compos Sci Technol 2001, 61, 2481–2490.

6. Shiao, M. L.; Nair, S. V.; Garrett, P. D.; Pollard, R. E. Polymer 1994, 35, 306–314.
7. Nair, S. V.; Wong, S. C.; Goettler, L. A. J Mater Sci 1997, 32, 5335–5346.
8. He, J.; Zhang, H.; Wang, Y. Polymer 1997, 38, 4279–4283.
9. He, J.; Wang, Y.; Zhang, H. Compos Sci Technol 2000, 60, 1919–1930.
10. Pisharath, S.; Wong, S. C. Polym Compos, in press.
11. Dutta, D.; Fruitwala, H.; Kohli, A.; Weiss, R. A. Polym Eng Sci 1990, 30, 1005–1018.
12. Isayev, A. I. In Liquid Crystalline Polymer Systems—Technological Advances; Isayev, A. I.; Kyu, T.; Cheng, S. Z. D., Eds.; American Chemical Society: Washington, DC, 1996.
13. Zhang, H.; Weiss, R. A.; Kuder, J. E.; Cangiano, D. Polymer 2000, 41, 3069–3082.
14. Kimura, M.; Porter, R. S. J Polym Sci Polym Phys Ed 1984, 22, 1697–1699.
15. Paci, M.; Barone, C.; Magagnini, P. L. J Polym Sci Part B: Polym Phys 1987, 25, 1595–1605.
16. Wunderlich, B. Macromolecular Physics: Crystal Melting; Academic: New York, 1980; Vol. 3, Chapter 9.
17. Nishi, T.; Wang, T. T. Macromolecules 1977, 10, 421–425.
18. Zheng, S.; Huang, J.; Li, Y.; Guo, Q. J Polym Sci Part B: Polym Phys 1997, 35, 1383–1392.
19. Gopakumar, T. G.; Ponrathnam, S.; Lele, A.; Rajan, C. R.; Fradet, A. Polymer 1999, 40, 357–364.
20. Ahn, T. O.; Hong, S. C.; Jeong, H. M.; Lee, S. W. Polymer 1996, 37, 3559–3565.
21. Huang, C. C.; Chang, F. C. Polymer 1997, 38, 2135–2141.
22. Costa, G.; Meli, D.; Song, Y.; Turturro, A.; Valenti, B.; Castellano, M.; Falqui, L. Polymer 2001, 42, 8035–8042.
23. Paul, D. R.; Barlow, J. W.; Keskkula, H. In Encyclopedia of Polymer Science and Engineering; Mark, H. F.; Bikales, N. M.; Overberger, C. G.; Menges, G., Eds.; Wiley: New York, 1989; Vol. 12.
24. Seo, Y.; Hong, S. M.; Kim, K. U. Macromolecules 1997, 30, 2978–2988.
25. Seo, Y. J Appl Polym Sci 1997, 64, 359–366.
26. Vallejo, F. J.; Eguiazabal, J. I.; Nazabal, J. Polym Eng Sci 2001, 41, 1115–1123.
27. Tjong, S. C.; Meng, Y. Z. Polymer 1997, 38, 4609–4615.
28. Chiou, Y. P.; Chiou, K. C.; Chang, F. C. Polymer 1996, 37, 4099–4106.
29. Isayev, A. I.; Modic, M. Polym Compos 1987, 8, 158–175.
30. Nylon Plastics Handbook; Kohan, M., Ed.; Hanser: Munich, 1994; Chapters 4 and 5.
31. Vasanthan, N.; Salem, D. R. Mater Res Nov 2001, 4, 155–160.
32. Bafna, S. S.; Sun, T.; De Souza, J. P.; Baird, D. G. Polymer 1995, 36, 259–266.
33. Campoy, I.; Gomez, M. A.; Marco, C. Polymer 1998, 39, 6279–6288.
34. Young, R. J. Introduction to Polymers; Chapman & Hall: London, 1983; Chapter 4.
35. Murthy, N. S.; Curran, S. A.; Aharoni, S. M.; Minor, H. Macromolecules 1991, 24, 3215–3220.
36. Ramesh, C.; Keller, A.; Eltink, S. J. E. A. Polymer 1994, 35, 2483–2487.
37. McCullagh, C. M.; Blackwell, J.; Jamieson, A. M. Macromolecules 1994, 27, 2996–3005.